CHALMERS

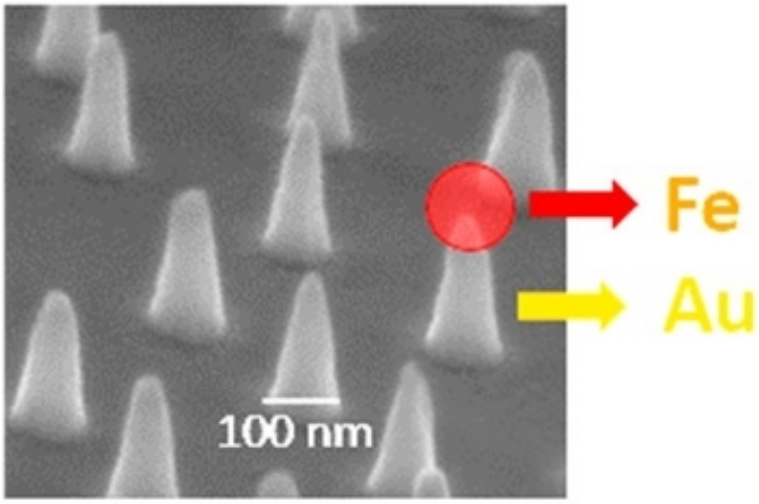

Nanoferromagnets in the focus of plasmon nanoantennas

Thesis for Erasmus Mundus Master of Nanoscience and Nanotechnology

LAVINIA GHIRARDINI

Department of Applied Physics
Chalmers University of Technology
Gothenburg, Sweden 2014

Education and Culture
Erasmus Mundus

KU LEUVEN

Thesis for the Erasmus Mundus Master of Science in Nanoscience and Nanotechnology, Nanoelectronics track

Nanoferromagnets in the focus of plasmon nanoantennas

LAVINIA GHIRARDINI

Promoter: Assoc. Prof. A. Dmitriev, Chalmers T.H.
Co-promoter: Prof. M. Heyns, K.U.Leuven

Department of Applied Physics
Chalmers University of Technology
Gothenburg, Sweden 2014

Nanoferromagnets in the focus of plasmon nanoantennas

LAVINIA GHIRARDINI

Department of Applied Physics
Chalmers University of Technology
SE 412 96 Gothenburg, Sweden
Telephone: +46 (0)31-772 10 00
Website: www.chalmers.se

Chalmers Reproservice
Gothenburg, Sweden 2014

To my family

Abstract

Plasmonics is the field of science that studies light-matter interaction. Collective oscillations of electrons at the surface of metals, resulting from an electromagnetic excitation, are responsible for plasmonic phenomena. In metallic nanostructures, these oscillations confine and enhance an electromagnetic field at a sub-wavelength scale, thus having a huge impact on enhanced sensing and spectroscopy applications. Moreover, plasmonics has been also used to enhance weak magneto-optical (MO) effects in magnetic materials. Magneto-optical phenomena are interactions between a magnetic field in a medium and an electromagnetic wave propagating through it [1], resulting in a rotation of the polarization plane and a change in the ellipticity of the polarization state. Magneto-optically active materials have nowadays found applications in a variety of contexts, such as magnetization imaging [2], telecommunication [3], sensors and data storage [4].

Current research focuses on the development of materials with large MO activity to improve the performance of these devices and expand their applications. Since an important factor in integrated technology is size, scaling the dimensions of MO components while preserving the readability of their signal is a crucial requirement. Since the MO response of a material is related to the optical field inside it, plasmonics can allow for its control and manipulation. The interplay between plasmons and magneto-optically active elements has been an important research topic in the field of magnetoplasmonics [5, 6]. Driven by such a research trend, fast, reliable and sensitive MO characterization tools are required in magnetoplasmonics. Conventional systems like the MOKE optical setup, based on frequency modulation methods, are expensive and rather time consuming [7]. This is especially cumbersome in the investigation of small signals which require, in addition, long detector integration time.

Here we develope a simple, fast, sensitive and broadband spectrometer-based plasmonic and MO characterization tool. With this tool, which allows small MO signal detection from nanostructures in ambient conditions [8], we study hybrid Au-Fe magnetoplasmonic nanoantennas with different compositions. Evolution of the MO signal when changing the relative amount of the two materials is assessed. We study the extinction spectra and MO response of both the pure Au and hybrid Au-Fe magnetoplasmonic systems. The trend studied is also compared to that of continuous Fe reference films. Our aim is to assess whether these hybrid structures, combined with the use of our detection scheme, are suitable to provide the reduction of the size of the magneto-optical active material without losing the ability to read MO signal from these nanostructures.

Keywords: magnetoplasmonics, nanoantenna, nanoferromagnet, Faraday rotation.

Acknowledgements

First, I would first like to thank my supervisor Prof. Alexander Dmitriev, for giving me a place in his group with this project and for showing always a contagious enthusiasm in everything he does. I must also thank my daily supervisor Dr. Addis Mekonnen, for his constant help and encouragement with my work and for his optimism and faith in the fact that results would finally arrive.

Thanks also to the rest of our small group Kristof Lodewijks, Irina Zubritskaya, Ines Massiot, Gustav Edman, and also to Ruggero Verre, for their help with fabrication and characterization training and problem solving. I am also extremely grateful to Matteo Savoini from Radboud University in Nijmegen and Randy Dumas from Gothenburg University in Gothenburg for their contribution to my thesis work.

I extend my thanks also to Prof. Guido Groeseneken, Prof. Göran Johansson and Ms. Elke Delfosse for their effort in organizing this Erasmus Mundus Master program, which is a wonderful experience from both an academic and a personal standpoint. I finally thank Prof. Marc Heyns for accepting to be my co-promoter at K.U. Leuven.

Thanks to all my friends from the program, especially the Göteborg group, for having been my family abroad during the past two years! I also thank my Italian friends for their moral support from abroad, their gossip updates and for making me always feel welcome back and a little bit homesick!

Thanks to my sister Elsa for her never-failing motivational support during the past two years, especially during the discomforting moments of the experimental work. Thanks also to my vice-family Giorgio and Lela, for their constant enthusiasm and support. Finally, last but not least, thanks to my wonderful parents, without whom none of this would have ever been possible.

Lavinia Ghirardini
Gothenburg
August 2014

Contents

1

Introduction

Plasmonics is a branch of optical condensed matter science aiming at studies of light-matter interaction [9]. The term "plasmon" refers to a quantum for the collective oscillation of free electrons, alluding to their plasma-like behaviour under the influence of electromagnetic radiation. Plasmons have been unconsciously used by glassmakers throughout history for aesthetic purposes [10]. This is because a dispersion of metallic nanoparticles with dimensions close to the visible light wavelengths in a glass matrix produces bright colors, both in reflection and transmission [11]. A more scientific approach to this phenomenon started at the beginning of the 20^{th} century [12, 13]. Only in the 1950s, however, after it was linked to the excitation of conducting electrons creating plasma oscillations ("plasmons"), did research on "plasmonics" properly begin [14].
Recently, the role of plasmons in enhancing magneto-optical signals has drawn large attention [5, 6]. Magneto-optics studies the behaviour of light propagating through (or reflected from) a magnetized medium [1]. In materials supporting these types of effects, different light polarizations present different propagation properties. This results in a rotation of the polarization plane and a change in the polarization state from linear to elliptical, phenomena that are nowadays implemented in a wide range of applications. Plasmons are here used to increase the degree of polarization rotation/ellipticity of light, as a result of intertwined magneto-plasmonic effects.

1.1 Surface Plasmons

The plasma-like conduction electron oscillations, called "plasmons", can be confined at the surface of a material and can localize and confine an electromagnetic wave there. Surface Plasmons (SPs) (or, more precisely, surface plasmon polaritons, SPPs - quasi-particles that combine plasmons and photons) are then the electromagnetic radiation coupled to these collective oscillations, localized at an interface between two media with

permittivities of opposite sign such as, for example, a dielectric and a metal [15].
The existence of SPs is due to the dielectric function of metals ϵ_m having a negative real part in the low-frequency spectral region. This means that metallic conductors tend to expel and reflect electromagnetic radiation. However, to have pronounced and well-defined SP resonances, optical losses must also be small [9]. For a metal to be a good plasmonic material, then, it must fulfill in a certain frequency interval the conditions

$$Re\epsilon_m < 0, \quad Im\epsilon_m \ll -Re\epsilon_m. \tag{1.1}$$

Good contucting metals, such as Ag, Au and Al, are known for their excellent plasmonic properties.
SPs can be sustained by a wide variety of metallic structures, like thin films or nanoparticles, and can be classified into two main categories depending on the dimensions of the metallic object considered.

1.1.1 Propagating Surface Plasmons

At extended planar interfaces, Surface Plasmon Polaritons (SPPs) are the propagating plasmon modes [5].
As an SPP propagates along the surface, it loses energy to the metal due to absorption or scattering, thus having a finite propagation length. For the same reason, the electric field falls off evanescently perpendicular to the surface, both in the metal and in the dielectric, thus confinig these surface waves in the perpendicular direction [16]. The SPP penetration depth (skin depth) is then the distance over which the field falls off, and it is smaller on the metal side, on the order of 20 nm over a wide frequency range. Propagation length and skin depth are material dependent, since they relate to losses incurred during propagation.
SPPs wavelengths are smaller than that of the exciting light, resulting in large field confinement at the interface and therefore small propagation distances, due to increased damping. Confinement below the diffraction limit of half the wavelength in the dielectric can be achieved close to the SPP resonance frequency.
Due to their bound nature SPPs cannot be directly excited by light, but require also a change in momentum. Coupling of photons into SPPs requires the use of special phase-matching techniques, such as grating or prism coupling, to match the photon and surface plasmon wave vectors.

1.1.2 Localized Surface Plasmons

Discrete entities, with dimensions on the order of or smaller than the wavelength of the exciting radiation, can sustain Localized Surface Plasmons (LSPs) [17]. They arise because the free electron cloud of a metal can be resonantly excited by an electromagnetic field at specific wavelengths, due to an enhancement in the nanostructure's polarizability.

This intensified polarizability gives rise to strongly enhanced near-fields at the metal-dielectric interface, in spatial regions referred to as hotspots, as shown in figure 1.1(b) [15].

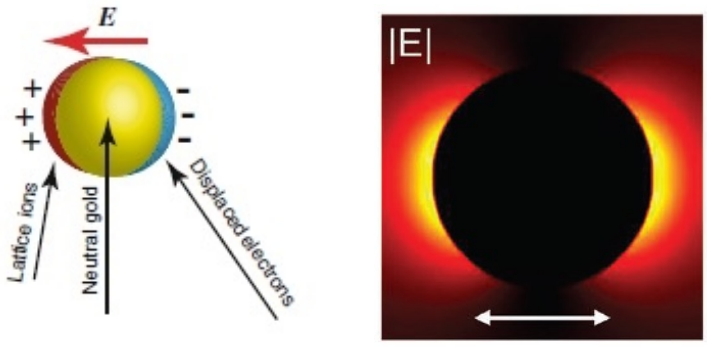

(a) (b)

Figure 1.1: Schematics of the charge oscillation of a LSP in a nanoparticle (a) and calculated field distribution for a nanodisk under LSP excitation (b). Images taken, respectively, from references [9] and [5].

Conduction electrons are weakly bound to their nucleus, allowing for charge fluctuations around the mean value (figure 1.1(a)). Such fluctuations generate electrostatic recoil forces aiming to recreate equilibrium conditions, thus inducing charge density oscillations. If the frequency of the incident radiation is in resonance with these oscillations, even a weak electromagnetic field can create strong LSP resonances (LSPRs). Since the latter are oscillating charge dipoles, they emit electromagnetic radiation in turn [18]. Consequently, the solution of the Laplace equation for the electric field in these structures consists of a superposition of the applied field E_0 and an ideal electric dipole located at the center of the structure, with dipole moment equal to

$$p = \alpha E_0 \tag{1.2}$$

where α is the complex polarizability of the metal nanostructure. For a nanoparticle of radius r smaller than the exciting wavelength, α can be approximated as

$$\alpha = 4\pi r^3 \frac{\epsilon_m - \epsilon_d}{\epsilon_m + 2\epsilon_d} \tag{1.3}$$

where ϵ_m and ϵ_d are the dielectric function of the nanoparticle and of its non-absorbing surrounding medium, respectively. This translates into a resonance condition for plasmonic excitation equal to

$$Re\epsilon_m = -2\epsilon_d, \qquad Im\epsilon_m \ll 0. \tag{1.4}$$

For large and complex nanostructures also higher order modes can be excited, given that the appropriate conditions are satisfied.
LSPR's enhanced near-field is highly localized at the nanostructure surface, within the skin depth, and decays rapidly away from the nanostructure-dieletric interface into the dielectric background. This light confinement down to subwavelength dimensions goes beyond the diffraction limit, and it is limited only by the size of the nanostructures [18]. Far-field scattering by the particle is also enhanced by the resonance [19].

With increasing dimensions of the nanoparticles, plasmon resonances show a red shift and an increase in their Full Width Half Maximum (FWHM). The latter happens because the decay of SPs occurs both via non-radiative and radiative paths. Consequently, since the radiative rate is proportional to the volume of the system, larger nanostructures present a shorter plasmon lifetime. As the size of particles increases, in fact, coherent electron oscillations become progressively more difficult, leading to an increase in scattering [9].

To summarize, surface plasmon resonance conditions depend on the refractive index of the surrounding media, on the geometry of the plasmonic nanostructures and on the permittivity of their material, as shown by equations 1.1 and 1.4 [17]. By playing with these parameters it is possible to tune the frequency of the plasmonic modes from the ultraviolet up to the near infra-red part of the spectrum. Moreover, SPs sensitivity to the optical properties of the surrounding dielectric medium has made them useful tools in biochemosensing applications [20, 21].

Plasmonic Nanoantenna

Near-field localization and enhamcement also increases the efficiency of light interaction with molecules or emitters located within the hotspot. In fact, a molecule situated in the near-field of a metal plasmonic nanosystem only weakly interacts with the external optical field but with the local one present at its position. Consequently, the local field enhancement causes an intensification of the radiative and non-radiative processes in which such a molecule participates [9].
This effect is often referred to as the nanoantenna effect, in analogy with the common radio-frequency antennas, and it is responsible for phenomena such as surface-enhanced

Raman scattering [22] and enhanced fluorescence emission [23]. Finally, other phenomena that this time depend on the externally applied magnetic field, such as magneto-optical effects, can be enhanced by LSPR resonances [5].

1.2 Magneto-Optics

Magneto-Optic (MO) phenomena are magnetic field-induced modifications of the optical properties of a medium [4]. In materials supporting these types of effects, called gyrotropic or gyromagnetic, different light polarizations present different propagation properties. Experimental evidence of magneto-optic phenomena was first reported by Michael Faraday in 1845 [24], who detected a change in the polarization state of transmitted light when a magnetic field was applied to a transparent glass. This type of phenomenon is thus called Faraday effect [4]. Similarly, a change in the polarization state of light that is reflected from a magnetized material is named Kerr effect, after John Kerr who first reported it in 1875 [25, 26].
The practical result of these interactions is that the plane of polarization of incident linearly polarized light is rotated, and the polarization state of the beam changes from linear to elliptical.

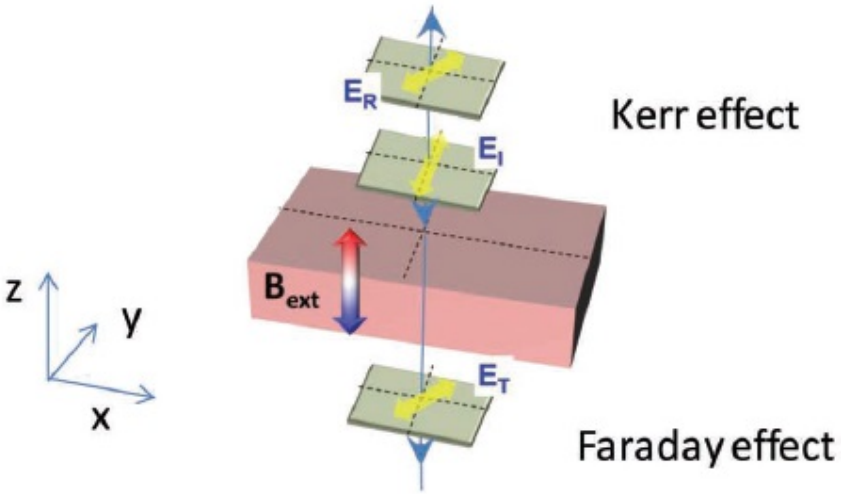

Figure 1.2: Illustration of the MO effects both in reflection and transmission, which are known as Kerr and Faraday Effects, respectively [5].

1.2.1 Faraday and Kerr Effects

To explain magneto-optical effects from a macroscopic point of view we look at the response of a material to an incident electromagnetic wave. It can be described in terms

of the electric displacement D by Maxwell's law [1]

$$D = \epsilon E \tag{1.5}$$

where ϵ is the electric permittivity of the material and E is the applied electric field. The parameter ϵ is frequency dependent and, in general, complex.
For a three dimensional non-magnetic and not optically active material, the electric permittivity is the tensor

$$\epsilon_\omega = \begin{pmatrix} \epsilon_{xx} & 0 & 0 \\ 0 & \epsilon_{yy} & 0 \\ 0 & 0 & \epsilon_{zz} \end{pmatrix} \tag{1.6}$$

where $\epsilon_{xx} = \epsilon_{yy} = \epsilon_{zz}$ if the material is isotropic, while the ϵ components assume different values along the different symmetry axes for the anisotropic case. Under the presence of a magnetic field, however, the permittivity tensor of magnetic materials becomes a non-diagonal matrix

$$\epsilon_\omega = \begin{pmatrix} \epsilon_{xx} & a\Pi_z & a\Pi_y \\ -a\Pi_z & \epsilon_{yy} & -a\Pi_x \\ -a\Pi_y & a\Pi_x & \epsilon_{zz} \end{pmatrix} \tag{1.7}$$

where $a\Pi_i = \epsilon_{mo}$ represents the MO constant of the material, with Π_i being the components of the applied magnetic field (for paramagnetic and diamagnetic materials) or the magnetization of the material (for ferromagnetic ones)[5]. We can also observe that the external magnetic field acts in a way that depends on its alignment with the material. In fact, the non-diagonal terms are activated when the medium is magnetized perpendicularly to the plane where they are defined.

In the quantum mechanical description, this effect is attributed to the spin-orbit interaction. The latter describes the energy of interaction of an electron's spin moment μ with its orbital momentum [27]. As this electron moves with momentum p through the electric field $-\nabla V$ generated by all the other electrons bound to the atom, it experiences an effective magnetic field $B = p \times \nabla V / m_e c^2$, where m_e is its mass and c is the speed of light. The spin-orbit interaction, then, has the form $\propto \mu \times \nabla V \cdot p$ and can be thought of as an effective magnetic field of vector potential $\propto \mu \times \nabla V$ acting on the motion of the electrons. This motion of charges gives rise to an electric current inside the material, thus affecting its optical properties. Such influence is a consequence of the fact that

the spin-orbit interaction causes shifts in the atomic energy levels, and will be further described in section 2.1.

The complex off-diagonal terms in 1.7, linking the magnetic field to the incident light polarization, are responsible for the Faraday and Kerr MO effects. Consequently these phenomena depend on the relative orientation between the magnetic field and the plane of incidence of light, and on the frequency ω of the incoming light beam [5].
This principle allows the study of the magnetization state of a material by looking at the change in the polarization state of light traveling through it, by means of Magneto-Optical Kerr or Faraday Effect (MOKE or MOFE) measurements [2]. The magnitudes experimentally explored are then the induced rotation θ and ellipticity ψ experienced by a beam reflected from or transmitted through a magnetic medium.

2

Magnetoplasmonics

MAGNETOPLASMONICS IS THE STUDY OF SYSTEMS in which magnetic and plasmonic properties are intertwined, either within the same material or in a combination of pure plasmonic and pure magnetic systems [5].

The nanostructured quasi free-electron metals, such as Au, Al and Ag, are among the best plasmonic materials. However, magnetic field assisted control and manipulation of light using such plasmonic structures is not a very efficient approach, due to their extremely weak MO response. On the other hand, the use of pure ferromagnetic nanostructures is not a viable approach either, since those materials are, in turn, very poor plasmonic candidates. By exploiting the combined properties of hybrid plasmonic and ferromagnetic nanostructures, magnetoplasmonics is foreseen to play a relevant technological role in different areas, such as integrated optics and data storage [28].

As plasmon resonances give rise to considerable localized field enhancements in the near-field of a nanostructure, the interaction of materials with externally applied magnetic fields is strongly enhanced. This results in a large increase in observed Kerr or Faraday rotation when measuring at the plasmon resonance wavelength [29].

2.1 Light Polarization Rotation

Every material exhibits MO activity, although its strength depends on its magnetic nature. The dimensionless magnetic susceptibility constant χ, which describes the response of a material to an applied magnetic field, is defined as

$$M = \chi H \tag{2.1}$$

where M is the magnetization of the material and H is an externally applied magnetic field. χ is a small positive and small negative constant for paramagnetic and diamagnetic materials, respectively. However, it has large and positive values for ferromagnets [4]. Paramagnetic and diamagnetic materials exhibit a linear dependence of the magnetization with magnetic field, while for ferromagnetic ones a saturation state can be reached. Moreover, the MO constants of ferromagnets are usually orders of magnitude larger than those of paramagnets and diamagnets [30].

When considering ferromagnetic materials, Faraday and Kerr effects are proportional to the net magnetization of the sample and independent on the strength of the externally applied magnetic field. They are connected with the ferromagnetic properties of the material. In fact, MO effects vanish when the magnetic medium is heated above the Curie temperature for ferromagnets [27]. The rotation angle is, in the simplest case, defined as

$$\theta = V dB \tag{2.2}$$

linearly proportional to the magnitude of the magnetic field B and the distance d travelled by light in the medium along the direction of the field. The proportionality constant is the Verdet constant V defined as the rotation per unit path, per unit field strength. This constant depends on the medium's properties, frequency of light, and temperature [1].

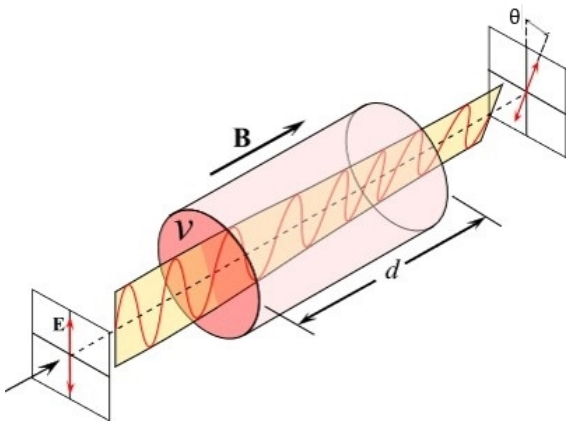

Figure 2.1: Faraday rotation of the polarization plane by an angle θ is directly proportional to the applied magnetic field B in the direction of light propagation and to the optical path d. The proportionality constant is the empirical Verdet constant V of the material [2].

This phenomenon is due to left and right circularly polarized waves propagating at different speeds through the material, property known as circular birefringence. Linear

polarization, in fact, can be seen as the superposition of two equal-amplitude circularly polarized components of opposite handedness and different phase. The result of a relative phase shift, induced by circular birefringence, is that the orientation of the linear polarization of the wave rotates.

The magnetic-field-induced Larmor precession of electron orbits is the simplest mechanism to explain Faraday effects [1, 27]. A magnetic field induces a splitting of the energy levels of quantum states with different eigenvalues of the angular momentum, known as Zeeman Splitting. Instead of one eigenfrequency of the electron ω, two separate eigenfrequencies ω_+ and ω_- arise, corresponding to the right-hand and the left-hand circular oscillations of electrons when a magnetic field is applied to the medium. This results in a modification of the macroscopic refraction indices of the material for the two different helicities $n_+(\omega)$ and $n_-(\omega)$. The physical implication of this phenomenon is that right- and left-hand circularly polarized waves propagate within the material with different velocities, c/n_+ and c/n_-.

For absorbing magneto-optically active media, instead, the induced Faraday rotation can be explained by a different mechanism. Magnetically induced Circular Dichroism (MCD) is observed when a sample differentially absorbs left and right circularly polarized light (LCP and RCP) in a magnetic field parallel to the light beam. MCD occurs due to the magnetic interaction of an external field with the electronic charge within the sample, and results in a modification of the polarization state of light [31].
The change in absorption between LCP and RCP in the presence of an external magnetic field results from a perturbation of the states involved in the optical transitions responsible for light absorption. The external magnetic field can split degenerate electronic states (first order Zeeman effect) or mix together states that were separated (second order Zeeman effect). This may occur either in the initial or in the final states.
When the sample absorbs LCP or RCP light, an electron is excited from an occupied state to an unoccupied state with different Δm_j, with m_j being the the projection of the total angular momentum along a specified axis. However, when a photon of a certain helicity and energy excites an electron, the consequent electronic transition depends also on the spin of the electron. Since the transition probabilities from initial to final states are governed by selection rules ($\Delta m_j = \pm 1$) and the helicity of the incident light ($m_l = \pm 1$), LCP and RCP no longer interact equivalently with the magnetic material in the presence of a magnetic field.

2.2 Noble Metals

As already mentioned, noble metals possess optimal plasmonic properties, but present intrinsically weak MO responses. The optical and magneto-optical properties of these materials are determined in an extended spectral range by their conduction electrons, and thus are reasonably well described by the Drude model [32, 33]. Consequently, their

MO constants can be expressed as

$$\epsilon_{mo} = i\frac{\omega_c(\omega_p\tau)^2}{\omega[(1-i\omega\tau)^2+(\omega_c\tau)^2]}. \tag{2.3}$$

where τ is the electrons relaxation time, and ω_p and ω_c their plasma and cyclotron frequency, respectively. $\omega_p = \sqrt{Ne^2/\epsilon_0 m^*}$ and $\omega_c = eH/m^*$, where e is the electron charge, N the electronic density, H the applied magnetic field and m^* the electron effective mass. For noble metals, when the magnetic field is not extremely high, ω_c is much smaller than ω_p, producing very small MO constants [34]. For example, the values for Au are roughly three orders of magnitude smaller than those for ferromagnetic metals like Co [35].
In magnetoplasmonic systems, though, the optical properties constitute another important factor. In particular, optical losses are of great importance, since they mainly determine the quality of plasmonic response. From this point of view noble metals are excellent materials, characterized by low losses and being able to sustain well-defined plasmonic resonances [34]. On the other hand, ferromagnetic metals usually exhibit large ohmic losses and very broad plasmonic peaks, but have a very good magneto-optical response [27]. Combining both materials in a hybrid nanostructure enables us to exploit both the plasmonic response of the noble metal nanoantennas and the MO effect of the ferromagnets.

2.3 LSP Effect on Polarization Rotation

As previously stated, magnetoplasmonics aims to produce an optimum combination of both MO and plasmonic characteristics within the same material or, by combining ferromagnets and noble metals. The ferromagnetic component provides the MO activity to the system, whereas the noble metal allows the SP excitation with low optical losses. This results in two main types of experimental research.
In active plasmonics, plasmonic properties are tuned upon the application of external stimuli, like temperature [36], voltage [37], photons [38] and magnetic field [39]. This aims to develop active components for integrated circuitry, like modulators, switches or sensors.
On the other hand, MO effects can be largely increased by plasmon resonance excitation, since the antenna effect produces an enhanced electromagnetic field in the region where the MO active component is located [6]. In this last case, the structures under study can be viewed as nanoantennas in the visible range with MO functionalities. This asset was chosen for our experiments, and it will be explained in more details in chapters 3 and 4.

3

Experimental Methods

By integrating plasmonic nanoantennas and ferromagnetic nanoparticles, we aim to increase the magneto-optical signal of the ferromagnetic nanoparticles. It is important to preserve the readability of magneto-optical signals when scaling down the dimensions of MO elements. Since the magneto-optical response of a material is proportional to the optical field inside it, plasmonics can allow for its control and manipulation. Thus, we use plasmonics as a tool to further scale down memory units and optical circuit components, and as a means to increase the sensitivity in detecting weak magnetic signals from ferromagnetic systems.

3.1 Sample Choice

The samples are Au truncated nanocones with ferromagnetic Fe conical tips at their apex. In order to observe their relative influence on the magneto-optical response, different proportions of the two materials have been considered. Three different magnetoplasmonic samples are investigated, all having a base diameter of about 100 nm and a total height of 210 nm.

Au height [nm]	Fe height [nm]
180	30
190	20
200	10

3.1.1 Antennas Optical Response

Au conical structures have been chosen as the plasmonic component due to the high degree of near-field confinement at their sharp tips [40]. Their geometrical structure also allows for the precise deposition of nanoparticles at the hotspots. In particular, these

structures posess two main plasmonic resonances. They are connected to the dipole oscillation along the in-plane and axial directions, which occur at different wavelengths as shown in figures 3.1(b) and 3.1(c).
By tuning the surrounding environment, dimensions of the nanocones, incoming light polarization and angle of incidence these two plasmonic modes can be separated or merged, according to experimental needs, and the overall nanocone's activity can be tuned [40, 41].

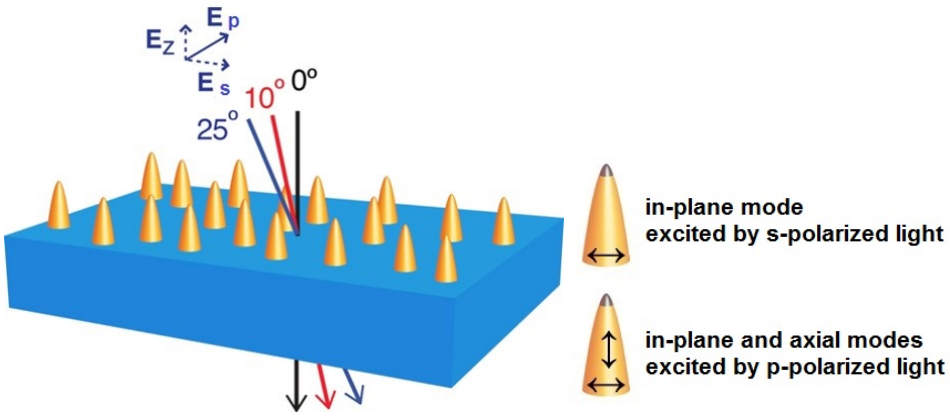

(a)

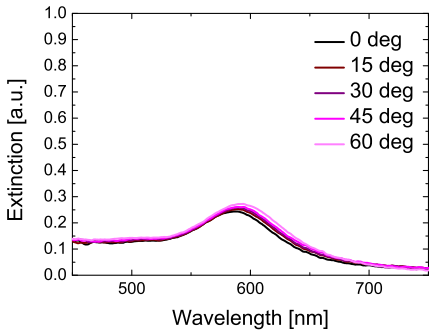

(b)

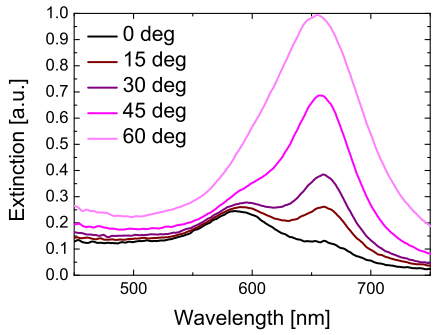

(c)

Figure 3.1: (a) Schematic illustration of the experimental geometry: Au nanocones with or without the Fe tip are randomly distributed over a glass slide, with the light beam of the spectrometer impinging on it. The setup is constructed so that the angle of incidence between the sample's normal and the light beam can be modified at will. Extinction response of the antennas to incoming s-polarized (b) and p-polarized (c) light as a function of the angle of incidence. In the first case, the peak shown corresponds to the excitation of the in-plane mode, while in the second they correspond to the excitation of the in-plane (lower wavelengths) and axial (higher wavelengths) modes. The samples shown in (b) and (c) are made of 170 nm tall Au antennas with 20 nm Fe conical nanoparticles on top.

Our samples are made of Au nanocones, with or without Fe tips, distributed with a short-range order (amorphously) on a glass substrate. The geometry of our experiment is shown in figure 3.1(a). The extinction response of the conical structures is also reported in figures 3.1(b) and 3.1(c), as a function of the polarization of the incoming light and of the angle between the incident beam and the sample's normal. The light beam is linearly polarized before reaching the sample and polarization can be either p or s, with the eletric field oscillating in the direction shown in figue 3.1(a).
Figure 3.2 shows Finite Difference Time Domain (FDTD) simulation of the field enhancement produced by our antennas upon illumination.

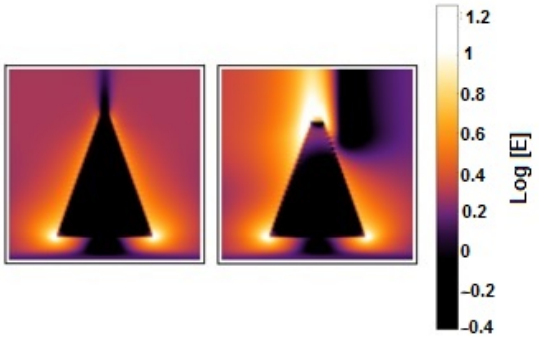

Figure 3.2: Finite Difference Time Domain (FDTD) simulations of the field enhancement produced by conical antennas when illuminated by a beam of wavelength equal to 700 nm. Incoming s-polarized light (left) excites the in-plane mode, resulting in field confinement at the base of the cones. Linearly polarized light with a component of the electric field oscillating along the cone axes (right) excites also the axial plasmonic mode. This results in a huge field confinement at the tip of the cone.

As we can see, incoming s-polarized light only excites the in-plane mode, resulting in field confinement mainly at the base of the cones. The excitation of this mode does not undergo significant changes when the angle of incidence is increased, due to the geometry of the system (figure 3.1(b)). Incoming p-polarized light, instead, excites both the in-plane and the axial modes, the latter being responsible for field confinement at the tip of the cones. In this case we notice a relevant dependence of the plasmonic response on the angle of incidence. This is because we move from an excitation of the in-plane mode only (at normal incidence) to the axial mode only (at grazing angle), passing through a series of geometries in which both modes are excited with the different strengths (figure 3.1(c)).
Since for our purpose the relevant hotspot is the one coinciding with the tip of the cones, all our experiments are conducted with incoming p-polarized light at a nonzero angle of incidence.

The last feature that must be mentioned is that our Au conical antennas present natural Circular Dichroism (CD). This property consists of the differential absorbance of left- and right-circularly polarized light (CD=$A_{LCP}-A_{RCP}$). Consequently, when linearly

polarized light passes through these conical structures its polarization state becomes elliptical, with the degree of ellipticity depending on the efficiency of CD generation from the nanostructures. The practical implication of this property in the frame of our experiments will be explained in section 3.3.2.

3.2 Fabrication Process

Our samples were prepared with the simple and inexpensive Hole-mask Colloidal Lithography (HCL) fabrication process [42]. This is a fast and low-cost technique, since the mask is formed through a self-assembly process which allows for the production of nanostructures over an area of several cm^2 and with a surface coverage that can go from 10% to 50%. As explained later on, the size distribution of the structures depends mainly on the size of the colloids used in the process. It is roughly 5% in case beads with diameter greater than 100 nm are employed, and goes up to 10% when smaller beads are used. The process steps are shown in figure 3.3.

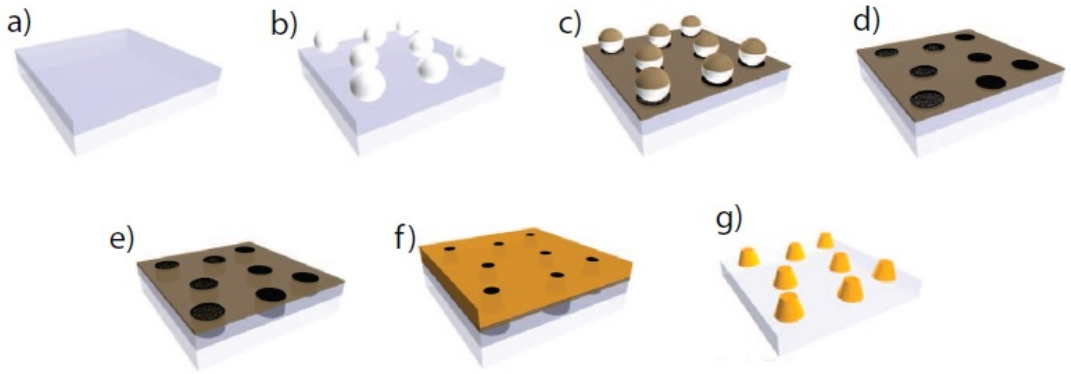

Figure 3.3: Overview of the HCL process: a sacrificial PMMA layer is spin coated on the substrate (a) and, after charged PS beads self-assemble on it (b), a metallic layer is deposited on top (c). The beads are then tape-stripped, thus revealing the mask pattern (d). The latter is transferred to the PMMA layer by oxygen plasma (e) and the chosen material is finally deposited through it (f). After lift-off of the PMMA with acetone under ultrasonication, the free standing nanostructures are revealed (g).

1. **Substrate pre-treatment.** Prior to processing, the substrate is cleaned by sonication at 50°C in acetone, isopropanol and de-ionized (DI) water, 5 minutes for each solution. The substrate used is glass (15x15 mm^2) or Si, depending on whether the sample is used for magneto-optical and optical characterization or for SEM imaging.
   A sacrificial layer of polymethylmethacrylate (PMMA) is spin-coated over the clean substrate. Spin coating of PMMA A4 (2%) at 3000 rpm for 1 minute produces a

layer of thickness of about 230 nm. The sample is subsequently baked for 10 min at 180°C to ensure solvent evaporation.

2. **Beads self-assembly.** The surface of the PMMA layer is then roughened by a 5 s oxygen plasma etch at 50 W, making the surface hydrophilic. Subsequently, the colloidal solution for the formation of the lithography mask is deposited. The sample is first covered with a polydiallyldimethylammonium (PDDA) solution at 0.2% wt for 30 s and then rinsed under DI water for an additional 30 s. After drying with a N_2 flow, a colloidal solution of polystyrene (PS) beads (2% wt) is deposited on the coated substrate for 2 minutes. The sample is again rinsed under DI water for 1 minute and then dried again.
   PDDA is a cationic polyelectrolyte which attracts electrostatically the negatively charged PS beads, keeping them on the sample. The final distance between the various nanostructures is determined at this step by the distance between the PS beads, which is determined in turn by their electrostatic repulsion.

3. **Mask definition.** A 10 nm Au film is deposited by evaporation. After this step the beads are tape-stripped, leaving parts of PMMA exposed through the Au layer and thus defining the features of the mask. Subsequently, 3 minutes oxygen plasma etch at 50 W ensure that the unprotected PMMA areas are completely etched through. Now the sample presents a lattice of holes that can be used as a mask to pattern the desired nanostructures.

4. **Material deposition.** We first evaporate a 1 nm thick Cr film as an adhesive layer for Au on the glass substrate by electron beam evaporation. The Au nanoantennas of 180, 190 and 200 nm height are then deposited on top of this layer by using the same evaporation technique. Electron beam evaporation is a physical process in which a conducting filament is heated to the point of thermal emission. The electron beam thus produced is then directed towards a metallic target, leading to material evaporation and consequent deposition on the sample. During the evaporation process, material deposition takes place not only through the holes but also on the mask, expecially on the edge of the holes. This causes a progressive decrease in their diameter, which produces a corresponding reduction of the dimensions of the structure evaporated through the holes. As shown in figure 3.4, this results in the definition of a conical shape [43].
   When the desired height of the plasmonic component is reached, the Fe nanoparticles are evaporated using the same mask. This ensures their exact deposition on the tips of the antennas, and defines their shape as conical as well.

5. **Lift-off.** When the process is complete, the mask is removed by lift-off in acetone, followed by rinsing in isopropanol and DI water.

Being the result of a self-assembly process, this technique is fast, relatively cheap and produces a large surface area coverage. Moreover, it is highly versatile in terms of the different types of structures that can be deposited by using the same type of mask, by simply changing the evaporation parameters and modality.

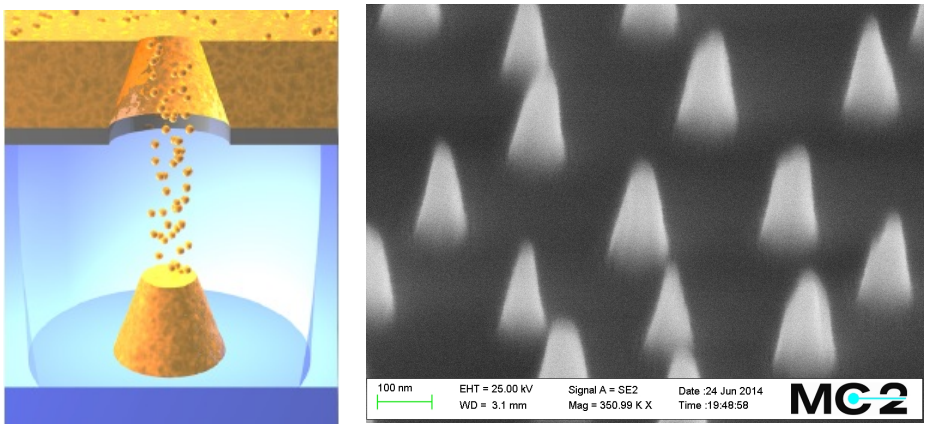

(a) (b)

Figure 3.4: Schematic of the deposition of a conical structure using the HCL process (a): geometry of the structure is produced by the progressive decrease in the mask-hole diameter, caused by material deposition on the hole's edge, adopted from [43]. SEM images of Au nanocones (b).

3.3 Experimental Setups

MO activity of the materials under study is usually small, typically less than 1°. When dealing with such small signals, then, a fast and ultrasensitive MO characterization is useful. Moreover, the signal detection becomes extremely difficult when dealing with magnetic nanostructures. In general, conventional MO detection systems must implement modulation and lock-in detection methods in order to extract weak signals from the background noise. Monochromatic laser light is then needed, since the modulation amplitude is wavelength dependent. As a consequence, these detection systems are not particularly sensitive but extremely time consuming, especially for the investigation of such small signals as the ones we deal with, which require in addition a long detector integration time [8]. Given the weak MO response expected from our samples, we require a sensitive, broadband and fast detection scheme.

3.3.1 Standard Magneto-optical Characterization Tools

Magneto-Optic Kerr Effect (MOKE) spectrometry is an experimental technique used to study the magnetic properties of thin films and multilayers. This technique is resonably sensitive and presents a simple and relatively lowcost setup [7]. MOKE measurements can be implemented with many different experimental geometries and setup components. In particular, the spectrometer present in our lab is a Longitudinal MOKE (L-MOKE) using a modulation technique. The schematic of a L-MOKE is shown in figure 3.5.

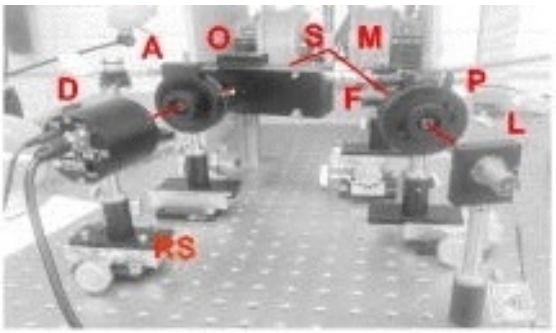

(a)

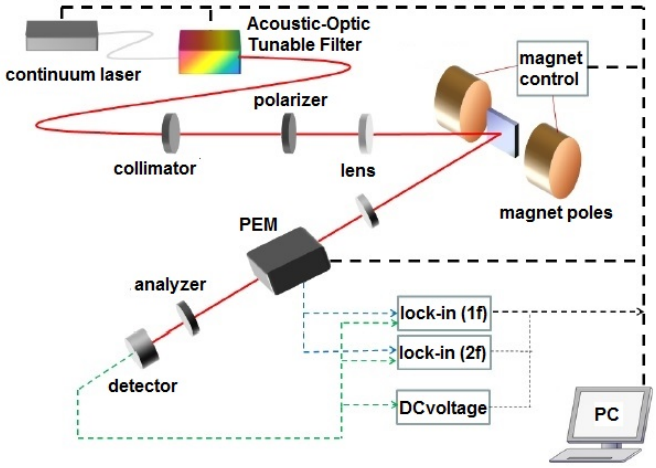

(b)

Figure 3.5: Picture (a) and schematic (b) of the structure of a L-MOKE spectrometer. The main components are the monochromatic light source (L), polarizer (P), focusing lens (F), sample (S), magnet (M), PEM (O), analyzer (A) and detector (D). The feedback loops of the lock-in amplifiers and the computer control of the system are also highlighted in (b).

Setup Components

A monochromatic light source is generated by a laser scanning all the frequencies in the UV-Vis-NIR range (roughly from 450 nm to 1200 nm). A wide spectral range is needed to cover all the possible resonance wavelengths of the plasmonic antennas. The optical elements consist of two polarizing prisms forming a crossed analyzer setup, a photoelastic modulator (PEM) and focusing lenses. The polarizer allows the selection of the light polarization incident on the sample, linearly p-polarized or linearly s-polarized. Light reflected from the sample, after traveling through it, is then elliptically polarized, with the major axis rotated with respect to the original polarization direction. This light polarization can be seen as the sum of two vectorial components, one parallel and one perpendicular to the optical axis of the PEM. The birefringence introduced by this

element makes it so that, at the given wavelength, one light component is alternately retarded and advanced by 90° relatively to the other, so that the exiting light is alternately right- and left-hand circularly polarized. The amplitude of this oscillation is adjusted by an externally applied voltage which is proportional to the wavelength of the light passing through the PEM. The modulation signals (its first and second harmonics) are used as references for lock-in amplifiers. Finally, the beam passes through the analyzer, which is set at 45° with respect to the polarizer, and is detected by a photodetector, providing the input signal to the lock-in amplifiers. In fact, the detected intensities at the fundamental and second harmonic of the PEM operating frequency depend, respectively, on the ellipticity and rotation introduced by the sample.

The signal is modulated at a high frequency and detected with lock-in amplifiers to exclude many sources of noise with frequency different from the PEM operating one (50 kHz) and to attenuate the white noise by the bandwidth of the lock-in amplifier. Lock-in amplifiers, in fact, provide large Signal-to-Noise ratios (SNR), thus facilitating the measurement of weak Kerr rotation in nanostructures. In order for them to be effective, though, the incoming signal must be modulated with a known reference frequency, which must be provided by the PEM. This component modulates the light at 50 kHz and generates two reference square wave signals: one oscillating at 50 kHz, used by one lock-in as the reference for the first harmonic measurement, the other oscillating at 100 Hz, to measure the second harmonic.

Such a detection setup presents few disadvantages. It relies on a complex detection scheme, which can be highly time consuming and not sensitive enough, especially for the detection of small signals. It also necessitates many electronics to control the various components, resulting in a fairly expensive and cumbersome setup.

3.3.2 Broadband Magneto-optical Spectrometer

To overcome the aforementioned disadvantages typical of MOKE magnetometers, we implement a detection scheme which follows directly the original experiment performed by Michael Faraday in 1845. Figure 3.6 shows a picture and a schematic of our new spectrometer. All optical components are mounted on a vibration-damped optical table.

Components and Mechanism

The light source is a Tungsten Halogen lamp (STE-SL1) with a wavelength range that goes from 350 nm to 1100 nm provided by StellarNet Inc [44]. For our experiments we use linearly p-polarized light, meaning that the electric field of the beam oscillates parallel to the incidence plane, we then set the transmission axis of the polarizer parallel to the table's surface (90°). The polarized light beam passes then through a diaphragm (D1), which isolates a narrow central part of the beam thus selecting as parallel rays as possible. The next optical element is a focusing lens (L1), which focuses the light beam

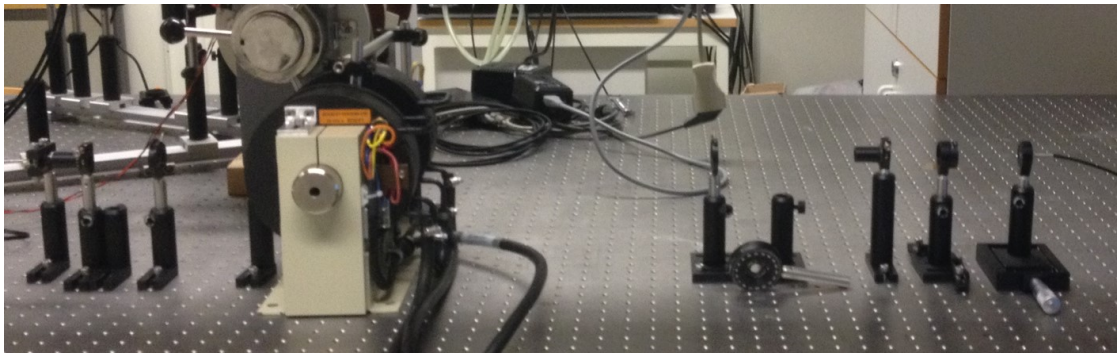

(a)

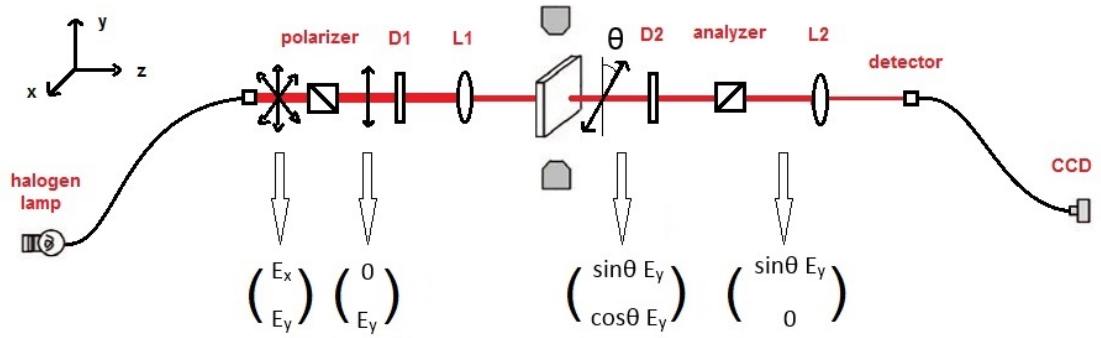

(b)

Figure 3.6: Picture (a) and schematic (b) of our broad band-optical spectrometer. The main components are the light source, polarizer, lenses (L), diaphragms (D), sample, electromagnet, analyzer and detector.

on the sample. A magnetic field up to 1 T can be applied to the sample with an electromagnet. The flexibility of our set-up allows us to vary the angle between the beam and both the sample's normal and the applied magnetic field. After passing through the sample, the beam is cut by another diaphragm (D2) and sent into the analyzer, whose transmission axis is crossed with respect to the polarizer's one. The polarizer and analyzer are Glan-Thompson prisms with 5 mm aperture. The outgoing beam is then collimated again through another focusing lens (L2) before reaching the detector. Light is fiber-coupled out from the source and into the spectrometer through fiber optic cables (STE-F600-UVVis-SR) connectors. Our spectrometer is a STE-SILVER-Nova from StellarNet Inc. (190-1100 nm) with a wavelength resolution of 0.5 nm. The detector is a 2048 pixel CCD, thermoelectrically cooled, using a miniature cosine receptor for UV-VIS-NIR (STE-CR2). Spectra recording is done with SpectraWiz software.

Matrix Analysis

Incoming light is unpolarized, with the electric field oscillating in all directions. It can be described by the general vector

$$E_{inc} = \begin{pmatrix} E_x \\ E_y \end{pmatrix}. \tag{3.1}$$

After passing through the polarizer only one component of the light vector is preserved, namely the one corresponding to the direction of the polarizer's axis. For example, following the schematics of figure 3.6, if light is polarized along the y direction only the E_y component is preserved

$$E_{inc} = E_y \begin{pmatrix} 0 \\ 1 \end{pmatrix}. \tag{3.2}$$

As stated in section 3.3.1, Faraday rotation is proportional to the magnetization of the sample. In fact, the magnetic medium acts on incident light by rotation its plane of polarization by an angle θ. This can be described by the matrix

$$S = \begin{pmatrix} cos\theta & -sin\theta \\ sin\theta & cos\theta \end{pmatrix}. \tag{3.3}$$

The overall transmission through the setup is then equal to the matrix product of matrix 3.3 with the polarization vector of the incident light beam 3.2 [7]. The electric field vector amplitude of the transmitted beam E_{out}, after passing through the sample, is then described by the following vector equation

$$E_{out} = E_y \begin{pmatrix} cos\theta & -sin\theta \\ sin\theta & cos\theta \end{pmatrix} \begin{pmatrix} 0 \\ 1 \end{pmatrix} = E_y \begin{pmatrix} -sin\theta \\ cos\theta \end{pmatrix}. \tag{3.4}$$

Since the analyzer is crossed with respect to the polarizer, the only component reaching the photodetector is the one along the x-direction. This leads to

$$E_{out} = E_y \begin{pmatrix} -sin\theta \\ 0 \end{pmatrix}. \tag{3.5}$$

The rotation signal recorded, considered as the intensity measured at the detector, is then proportional to the square modulus of the transmitted electric field vector $|E_{out}|^2$

$$I \propto |E_{out}|^2 = (E_y sin\theta)^2. \tag{3.6}$$

Since the rotation angle θ is small, typically of the order of millidegrees, sinθ can be approximated by the angle itself ($sin\theta \approx \theta$). Light intensity is then approximatively equal to

$$I \propto |E_{out}|^2 = (E_y \theta)^2 \tag{3.7}$$

where the information regarding Faraday rotation is stored in the rotation angle θ. If no magnetic medium or a non magneto-optical active one is present between polarizer and analyzer, no rotation is introduced. If $\theta = 0$, then, no light reaches the photodetector. Instead, if $\theta \neq 0$, light will reach the photodetector in a quantity proportional to the amount of rotation introduced.

Optical Measurements

To perform optical measurements, the analyzer is removed. The measured quantity is the extinction signal provided by the samples, which corresponds to the sum of their transmission and of the light scattering they induce.
The spectrometer is used in this conformation to perform the optical characterization of the plasmonic nanoantennas and to assess the extinction contribution of the ferromagnetic elements in the different samples. The reference signal is taken as the extinction of a glass slide at the same incoming polarization and incidence angle which will then be used for the samples. To assess the ferromagnetic tip contribution the extinction of the pure Au antennas is used as reference. The detector integration time used is 5 s. A lower integration time could also be employed, since increasing the latter merely reduces the SNR without changing the extinction pattern.

Magneto-optical Measurements

To perform magneto-optical measurements, the analyzer is used to filter the outgoing light from the sample. As it is cross-polarized with respect to the polarizer, it selects only the light component produced as a result of the rotation induced by the magneto-optically active sample. Since the Au nanoantennas exhibit intrinsic circular dichroism (see section 3.1.1), it is impossible to completely extinguish their extinction signal with cross polarizers. As a measure of this condition, the reference signal is then taken as its

minimization, corresponding to the crossover point between two very different shapes of the photon count image of the detector.

The reference signal is taken as the extinction of the sample at zero applied magnetic field. An external magnetic field is then applied, inducing wavelength-dependent modifications in the absorption signal of the sample. The detector integration time used is 30 s and, to increase the SNR, three spectra are taken for each applied field polarization which are then averaged using the software Origin 8.
The result of such measurements is shown in figure 3.7. Figure 3.7(a) shows the Faraday rotation induced by the sample upon application of a magnetic field. The effect is not symmetric for the different field polarities. The derived Faraday rotation, shown in figure 3.7(b) can be then calculated as

$$\theta = \frac{I^{+}_{norm} - I^{-}_{norm}}{2} \tag{3.8}$$

where I^{+}_{norm} and I^{-}_{norm} correspond to the intensity of the signal upon application of, respectively, +B and -B. The subscript stands for the fact that the mentioned signal is normalized with respect to the zero applied field one.
The magnetic field is controlled by the voltage applied to the electromagnet. In our experiments fields up to roughly 1T were applied.

Comparison with MOKE Setup

In the definition of our new setup, we follow the original experiment of Michael Faraday. We implement direct polarized light absorption measurements as a simple, spectrally resolved, broadband, fast and flexible alternative to traditionally more complicated and time consuming magneto-optical detection schemes.
Some of the advantages provided by this approach are:

- Flexibility in terms of sample and magnetic field orientation. The angle between the light beam and both the sample and the magnetic field can be modified at will, according to the requirements of each experiment.
- Simpler setup preserving extremely high sensitivity. Our detection scheme does not require PEM modulation or lock-in techniques, but is still able to sense signals coming from very small entities (see section 4.2).
- Fast detection. By scanning all the wavelengths in parallel, roughly from 450 nm to 1100 nm, rotation measurements become less time consuming. This allows also the use of longer detection integration times, thus further increasing the SNR.
- Extinction and magneto-optic characterization using the same spectrometer, by simply adding or removing the analyzer between light source and detector. This aspect is extremely important when dealing with magnetoplasmonic systems like

the ones we consider, in which optical properties are highly dependent on the experimental geometry (see section 3.1.1).

On the other hand, when compared to a MOKE setup, our broadband-optical spectrometer has also a few disadvantages, which could be easily overcome with a few small adjustments:

- Does not give a magnetic hystersis loop instantly. To obtain this information one should record the rotation scan for various applied field values and then plot only the ones corresponding to the desired wavelength. This manual procedure can be easily automated with some programming and by introducing a remote magnetic field control.
- It is very senstive to room-light, and to other parameter changes. Before taking measurements one must perform a careful alignment and use a proper light-shielding. References to quantify the relative angles between the light beam, sample and magnetic field would make also the measurements more reproducible.

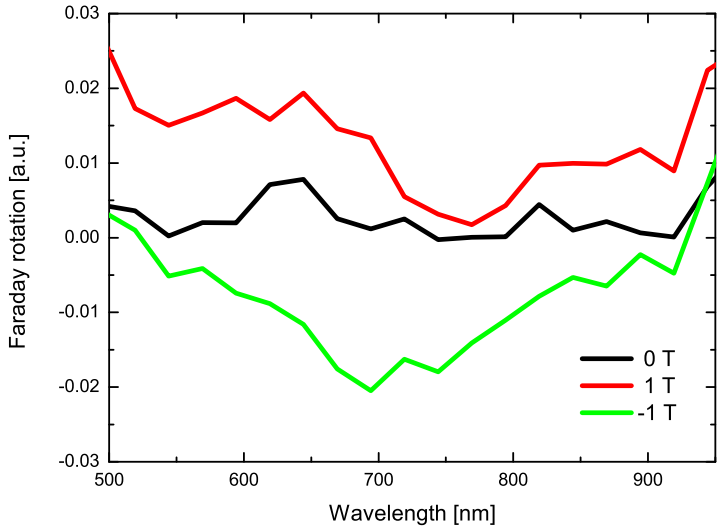

(a)

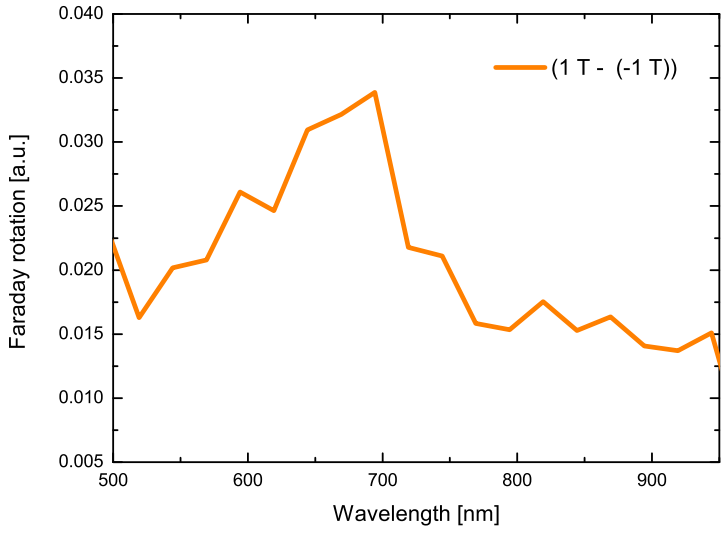

(b)

Figure 3.7: Result of a magneto-optical measurement performed with the new spectrometer. This particular spectrum has been taken from a sample composed of 170 nm tall Au cones with 40 nm Fe conical nanoparticles. Figure (a) shows the modification in Faraday rotation signal induced by the application of different values of magnetic field, while figure (b) shows the Faraday rotation signal extrapolated from the latter.

4

Results

Plasmonic and magneto-optical responses of our samples are characterized, in order to study the effect of the Au nanoantennas on the magneto-optical response of Fe nanoparticles positioned at their apex. The role of pure Au antennas on the extinction spectra of Fe nanoparticles, as well as the reverse effect, is assessed. We detect very weak magneto-optical signals by exploiting the enhancing effect provided by the Au nanoantennas. Without this amplification, the signals would be too weak to be detected using standard magnetization characterization tools such as an Alternating Gradient Magnetometer (AGM).

4.1 Plasmonic Response

The extinction spectra of the pure Au nanocones and of the hybrid Au-Fe nanocones, respectively, are shown in figures 4.1 (a) and (b). Tables 4.1 (c) and (d) list the position of the plasmonic resonance peaks and their Full Width Half Maximum (FWHM) for different heights of pure Au nanocones and with different Au-Fe proportions, respectively. Extinxction spectra have been taken with incoming p-polarized light at a nonzero angle of incidence.
Considering the pure antennas, we observe a red-shift in the peak position and an increase in its extinction value as the aspect ratio of the Au antennas increases. This trend is expected, since the amount of material involved in the plasmonic resonance is progressively increasing. As expected, also the FWHM of the peaks increases with increasing antennas height, as explained in section 1.1.2. Comparing tables 4.1 (c) and (d), we can see that the addition of the ferromagnetic tip not only induces a further red-shift in the peak position, but also slightly improves the quality of the plasmonic peaks by reducing their FWHM by a few nanometers. This last result is unexpected, since Fe is a poor plasmonic material and should thus deteriorate the quality factor of the plasmonic resonance.

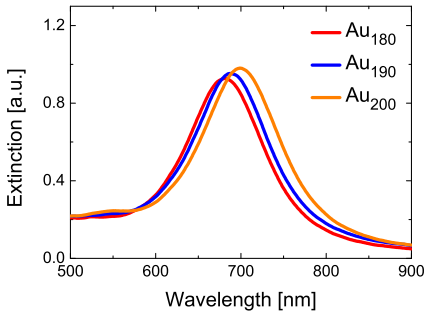

(a)

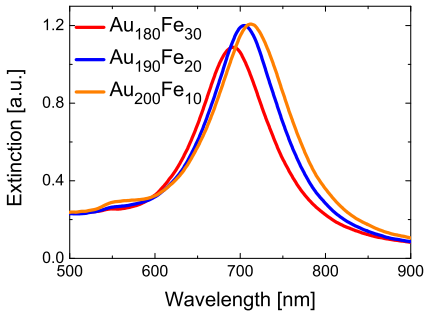

(b)

Sample	Peak [nm]	FWHM [nm]
Au_{180}	681	116
Au_{190}	687	117
Au_{200}	699	119

(c)

Sample	Peak [nm]	FWHM [nm]
$Au_{180}Fe_{30}$	692	109
$Au_{190}Fe_{20}$	704	111
$Au_{200}Fe_{10}$	712	117

(d)

Figure 4.1: Extinction spectra of the pure Au antennas (a) and of the combined Au-Fe systems (b) recorded using p-polarized light. In both cases, the resonance peaks show a progressive red-shift when the antennas height is increased. The values for the resonance peak position and FWHM for the pure Au antennas (c) and for the hybrid Au-Fe systems (d) are also listed.

Moreover, in the graphs presented in figure 4.1, an additional feature around 550 nm can be distinguished. This can be possibly identified as the plasmonic contribution deriving from the excitation of an higher order mode in the Au nanocones. Figure 4.2 looks closely at this feature from the Au and Au-Fe extinction spectra. It follows the trend described above, presenting an increase in the peak height and a red-shift in its position with increasing amount of plasmonic material.

Finally, we look at the extinction contribution by the ferromagnetic material only. This is done by taking the extinction spectra of pure Au cones as a reference signal to study the extinction pertaining to the ferromagnetic tips. These extinction curves do not correspond to the expected plasmonic contribution of the Fe tips. In fact, since this material has a very poor plasmonic response, given the particles dimensions, the corresponding broad peak should be present at relatively high energies, out of the visible range. Here we can argue than the Fe tip acts as a passive material within the spectral range considered. We therefore think that the resulting absorption pattern is a measure of the enhancement of the electromagnetic field induced by the pure plasmonic antennas at

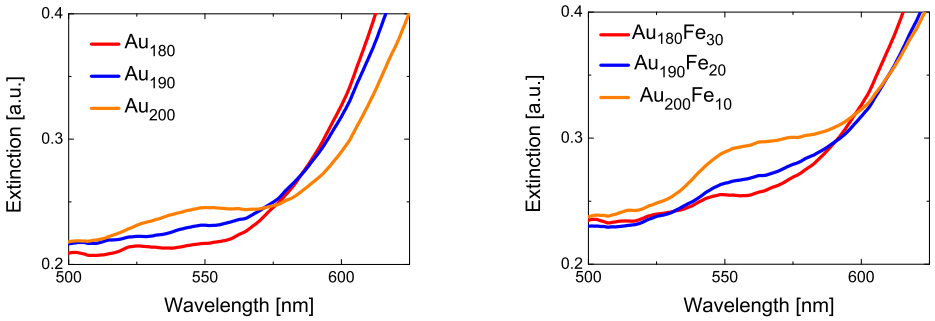

Figure 4.2: Extinction spectra of the pure Au antennas (a) and of the combined Au-Fe systems (b), which shows a further third mode in addition to the two modes described in section 3.1.1. The features represented correspond to the excitation of a higher order mode and follows the same trend as the dipole modes for the different samples.

their tip normalized to their height. FDTD near-field simulations were also performed by Matteo Savoini at Radboud University in Nijmegen, and are shown in figure 4.3. The latter shows an increase in the near-field intensity at the nanocones tip when the height of the Au cones increases from 180 nm to 200 nm and the one of the Fe tips decreases from 30 nm to 10 nm. In the FDTD simulations, we notice a slightly asymmetric field distribution, which we think might be due to the directionality in the illumination of the sample induced by the experimental geometry.

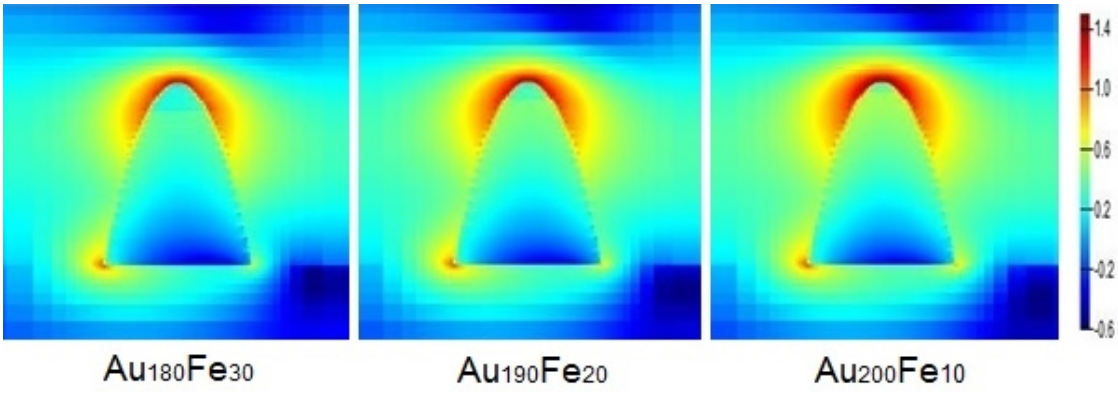

Figure 4.3: FDTD near-field simulations of the Au-Fe nanostructures. Extinction enhancement at the hotspot increases when moving towards taller antennas and smaller particles.

To give a further experimental insight, we replicate our measurement with a sample where the plasmonic component is replaced by a dielectric material (Al_2O_3), which should not provide any field enhancement. Consequently, since this system lacks the

plasmonic component, it should not present any MO-features enhancement (see figure 4.6).

4.2 Magneto-optical Effect

Figure 4.4 shows the Faraday rotation signals for continuous Fe films with the same thickness as the height of the Fe nanoparticles considered in section 4.1.

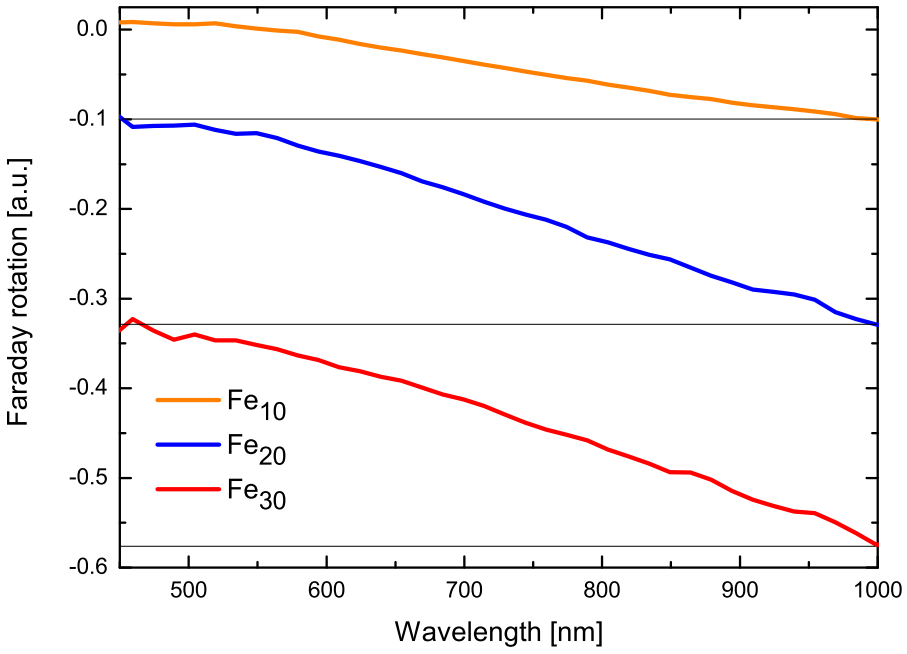

Figure 4.4: Faraday rotation signal of Fe films with thickness equal to the height of the nanoparticles.

We note that, when the thickness of the film increases, the magneto-optical Faraday rotation it induces also does, in accordance with the Verdet law. In fact, equation 2.1 states that the amount of rotation is proportional to the optical path within the magneto-optically active material. The trend observed in figure 4.4 is thus in agreement with our expectations.

Figure 4.5(a) shows the Faraday rotation signals for our three different magnetoplasmonic systems. We observe an amplification in the magneto-optical signal of the Fe nanoparticles characterized by a peak in correspondence with the plasmonic resonance

frequency of the antennas, where the field localization is maximized.

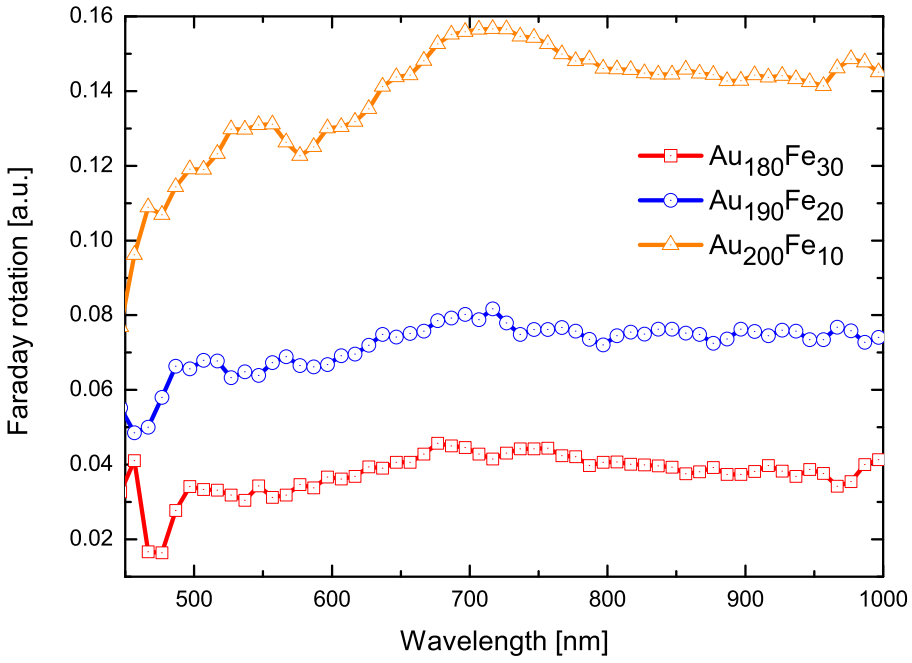

(a)

Sample	Main peak [nm]
$Au_{180}Fe_{30}$	700
$Au_{190}Fe_{20}$	713
$Au_{200}Fe_{10}$	718

(b)

Figure 4.5: Faraday rotation signal of the Au-Fe magnetoplasmonics systems (a). A vertical offset between the different data lines has been included to allow a better comparison of the signals. The position of the main rotation peak for the various systems is also listed (b).

Despite the smaller amount of ferromagnetic material, the signal strength and quality increase when moving from the $Au_{180}Fe_{30}$ to the $Au_{200}Fe_{10}$ samples. This indicates that the improvement in field enhancement and localization produced by taller plasmonic antennas efficiently compensate for the decrease in magnetic material. This is in agreement

with the FDTD simulations presented above. In fact, as a consequence of this, the signal of smaller particles is enhanced more than the one of bigger ones. This happens because taller plasmonic nanocones provide a higher near-field enhancement, as shown in figure 4.3.
Moreover, when moving to smaller particles, the rotation peak red-shifts (see table 4.5(b)) and the second feature at 550 nm becomes more pronounced. This behaviour also follows the trend of the plasmonic extinction response of the system, an additional confirmation of the fact that the observed rotation enhancement is due to the presence of the antenna.

4.3 Role of Au Nanocones

To confirm that the observed peaks come from an enhancement of the MO activity of the Fe nanoparticles, and not from the MO activity of the Au antennas, the rotation spectra of the latter is recorded.

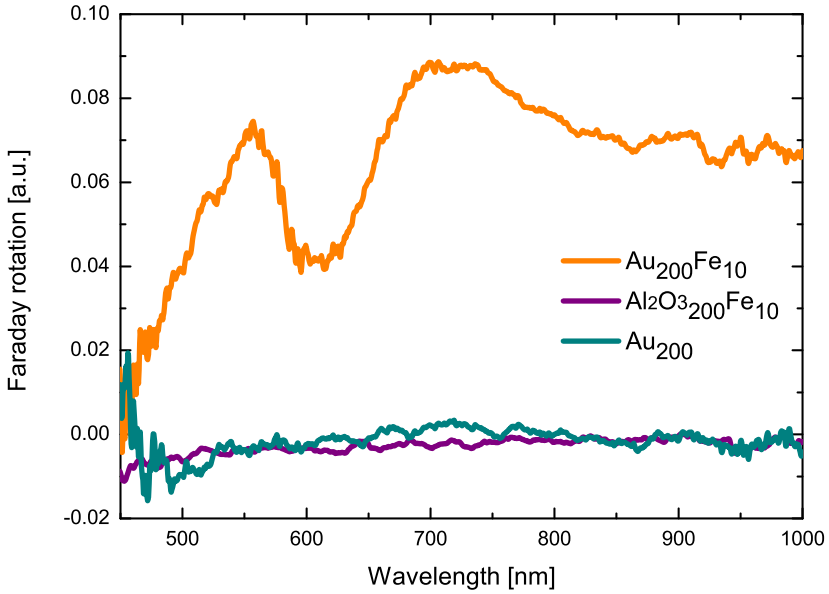

Figure 4.6: Comparison of the rotation signal of the Au-Fe magnetoplasmonic systems with the ones of the corresponding pure Au antennas and with the one of a system where the plasmonic component has been replaced with a dielectric. These results show that the rotation signal registered comes from the Fe nanoparticles, and that this small signal is readable thanks to the enhancement provided by the plasmonic antennas.

As figure 4.6 shows, the MO contribution of the plasmonic component is barely notice-

able, being limited to a small peak in correspondence with the plasmonic resonance.
Figure 4.6 also shows a comparison between the rotation signals of the magnetoplasmonic system with the one of 10 nm Fe tips on 200 nm high Al_2O_3 cones. As already mentioned in section 4.1, this is done to further confirm that the presence of a readable signal is made possible only by the presence of the Au plasmonic antennas.
The trend described in figure 4.5(a) can be then once more connected to the near-field localization and enhancement at the hotspot of the antennas. The higher the aspect ratio of the pure plasmonic antennas the more effective the consequent field intensification, resulting in a more enhanced Faraday rotation signal from the ferromagnetic tips.

4.4 SEM Characterization

To stress the sensitivity of our new spectrometer, we proceded with a statistical analysis of the sample showing the highest plasmonic-assisted MO rotation: the 200 nm high Au cones with 10 nm Fe tips. We calculate the average height and slant height of the cones by performing measurement over SEM images of our samples which, for this purpose, were prepared on a Si substrate to provide a better imaging contrast. The software ImageJ was used to perform the geometrical measurements. Figure 4.8 shows some of the images used for our evaluation.
Cone height and slunt height were calculated from the images considering a 45° angle between the samples and the imaging beam, and an average cone base of 100 nm. 60 different Au and Au-Fe nanocones have been taken into account for our statistics.
As an average result, we obtain a height value of 199.9 nm for the pure Au antennas and 211.8 nm for the complete system. Both these estimations are in perfect agreement with the parameters we set during material deposition.
To calculate the base radius of the Fe conical nanoparticles, we consider the complete system as an Au truncated cone with the remainig Fe cone on top. A model of the system in shown in figure 4.7, where "s" and "h" stand for "slant height" and "height", respectively.

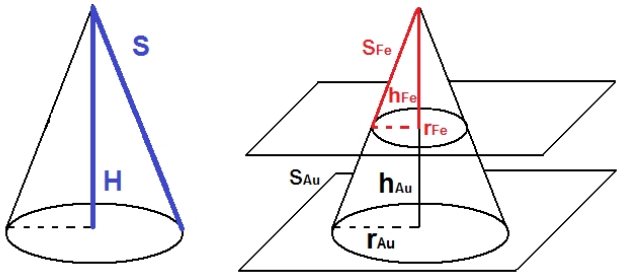

(a)

Figure 4.7: Model used to estimate the geometrical parameters of the $Au_{200}Fe_{10}$ cones. "s" and "h" stand for "slant height" and "height", respectively.

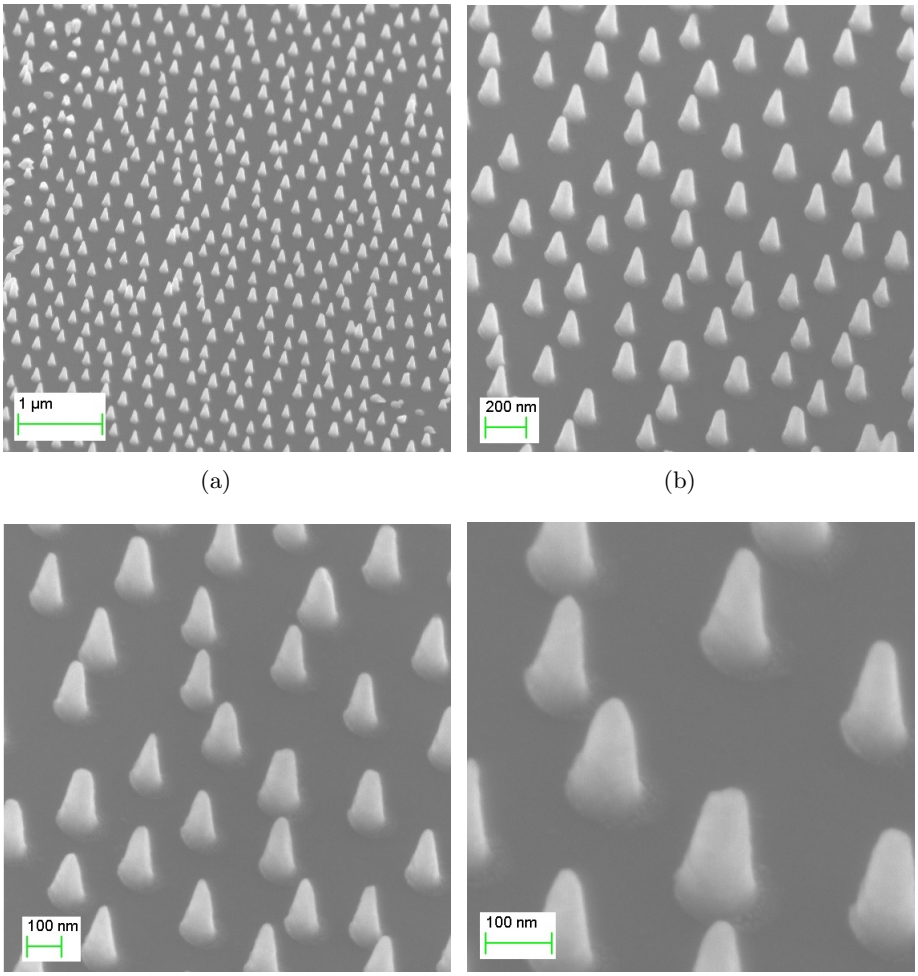

Figure 4.8: SEM images of the Au antennas and of the hybrid Au-Fe nanocones system at various magnifications. In order to get a good visualization with the electronic microscope the samples were grown on a silicon substrate.

The parameter measured from the pictures with ImageJ are S and s_{Au}, while r_{Au} is considered as equal to 50 nm on average and H is calculated from S as $\sqrt{S^2 - r_{Au}^2}$. The base of the Fe conical particle can be then computed with the corresponding solid geometry formulas when knowing the slant height of the two systems, the average base diameter and the height of the complete Au-Fe cone

$$r_{Fe} = \sqrt{s_{Fe}^2 - h_{Fe}^2} \tag{4.1}$$

where $s_{Fe} = S - s_{Au}$ and $h_{Fe} = H - h_{Au} = H - \sqrt{s_{Au}^2 - (r_{Au} - r_{Fe})^2}$. From these calculations we get, for the Fe conical tips, an average base diameter of 6.8 nm and an average height of 11.9 nm.

This results in a cone of volume equal to 145.8 nm^3 ($V_{cone} = \pi r_{Fe}^2 h_{Fe}/3$). The portion of sample contributing to the signal is the one illuminated by the incident light beam, which we estimate having a radius of $r_{beam} = 0.5$ mm, corresponding to an area $A_{spot} = \pi * r_{beam}^2 = 7.9e^{11}$ nm^2. The area occupied by each nanocone, instead is $A_{cone} = \pi * r_{Au}^2 = 7.9e^3$ nm^2. Considering a typical HCL coverage of 10%, we have roughly $N_{cones} = (A_{spot} * 0.1)/A_{cone} = 10000000$ cones contributing to the MO signal recorded. With a Fe density of $\rho_{Fe} = 7.874$ g/cm^3, this gives a mass of Fe equal to $m_{Fe} = V_{cone} * N_{cones} * \rho_{Fe} = 1.1479e^{-4}$ g.
This amount of material, if composing a continuous Fe film, would correspond to a film thickness of $h_{film} = m_{Fe}/(\rho_{Fe} * A_{spot}) = 0.0019$ nm. This means that, with the support of plasmonic nanoantennas and with our novel broad band-optical spectrometer, we detected a magnetization signal equivalent to the one provided by single atoms, positioned on the surface as a sub-monolayer.

4.5 Comparison with AGM technique

To further test the sensitivity of our spectrometer, we compare one of the results previously presented with the more traditional Alternating Gradient Magnetometer (AGM) magnetization detection technique, which does not exploit the antenna effect of plasmonic structures to enhance its signal. Figure 4.8 shows a typical AGM setup and its schematic.

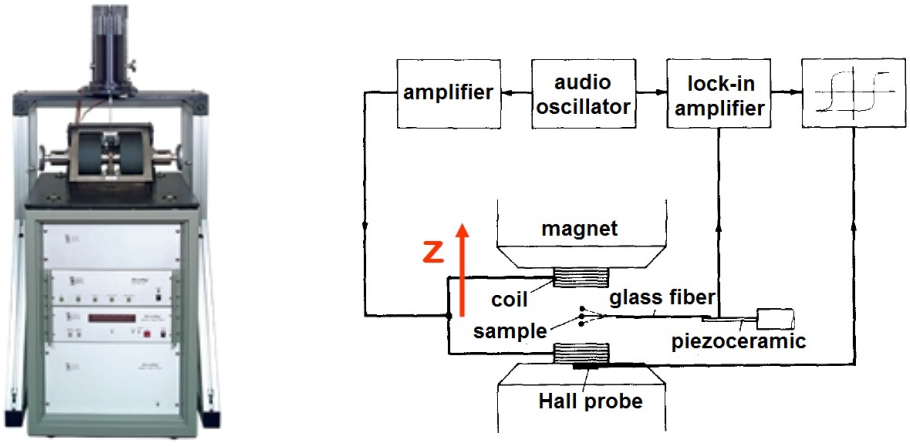

(a) (b)

Figure 4.9: Picture (a) and typical schematic (b) of an AGM magnetometer setup.

This tool determines the magnetic moment of a sample by measuring the force exerted on a magnetic dipole by a magnetic field gradient [45]. The sample is placed in a static magnetic field which is locally modified by a small varying field obtained by driving an alternating current through conducting coils. This creates a field gradient which exerts a sinusoidally varying force on the sample. This force is measured by a piezoelectric element which is connected to the sample by a glass capillary. The piezoelectric element creates a voltage proportional to the elastic deformation experienced by the sample and, hence, to the force acting on it. This technique presents a high sensitivity, which reaches up to 10^{-11} Am^2 (or 0.01 μemu) by using lock-in detection of the piezo voltage and by tuning the frequency of the field gradient to the mechanical resonance of the sample [46].

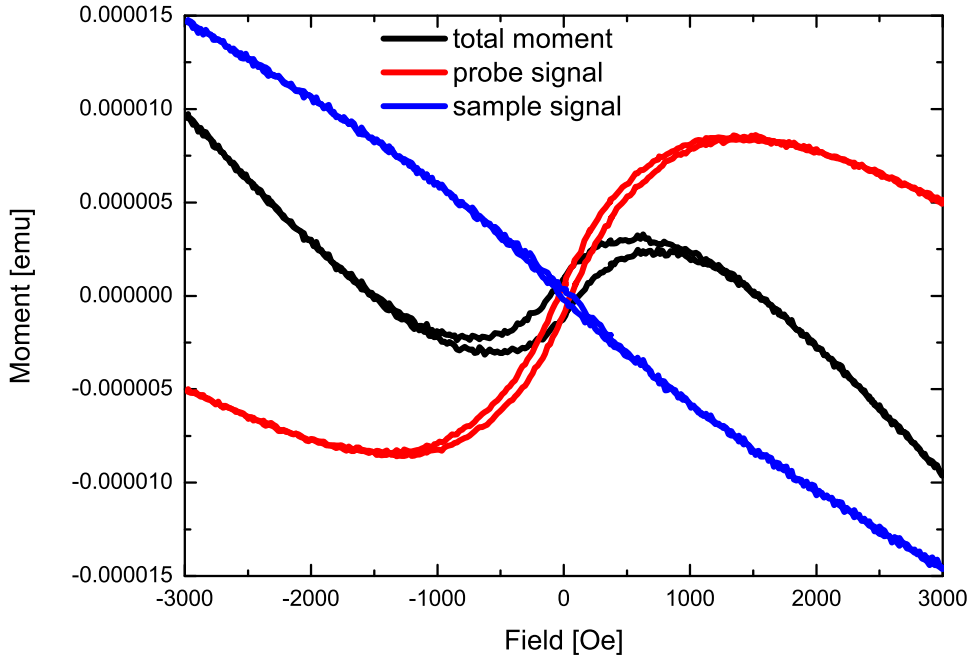

Figure 4.10: AGM measurement performed on the $Au_{200}Fe_{10}$ sample. The measured signal (black line) corresponds to the total signal of the system. It is the sum of the signals coming both from the probe (red line) and from the sample (blue line).

Figure 4.10 shows the AGM measurements performed on the sample $Au_{200}Fe_{10}$. The black line corresponds to the measured signal, which is the sum of the signals coming both from the probe (red line) and from the sample (blue line). The sample signal has been extrapolated as the difference between the total and probe signals.
From figure 4.10, we see that AGM measurements give no significant magnetic response for our structures other than a diamagnetic contribution due to the glass substrate. In

our magneto-optical measurements, though, we record a very strong signal for the exact same sample.
This means that our set-up is able to read magnetic signals from ferromagnetic entities so small that their magnetization cannot be detected with conventional high-resolution magnetometers. This happens because our detection scheme can exploit the signal intensification produced by the nanoantenna's near-field enhancement ability which is lacking in the AGM technique magnetization measurements.

5

Conclusions

In this thesis we investigated the magneto-optical signal of Fe nanoparticles with the assistance of plasmonic components, exploiting the antenna effect provided by the Au component. The plamonic antenna-assisted Faraday rotation signal was studied as a function of the relative amount of the pure plasmonic and pure ferromagnetic materials. We also implemented a new detection scheme which aims, by reverting to an experimental implementation more similar to the original Faraday demonstration of magneto-optical rotation, for easier and more sensitive signal recording.

Our experiments show that the detected rotation signal comes mainly from the Fe nanoparticles, with the Au antennas providing just a negligible contribution at their resonance frequency. Nonetheless, we also show that the presence of the plasmonic component is essential for the detection of the rotation signal coming from such small entities. Consequently, we confirmed that the plasmonic excitation of the Au antennas focuses the electromagnetic field at their hot spot, thus enhancing the magneto-optical activity of the Fe nanoparticles present at their tip. The rotation behaviour detected shows an amplification in the magneto-optical signal of the Fe nanoparticles characterized by a peak in correspondence with the plasmonic resonance frequency of the plasmonic antennas, where the field localization is a maximum.

By looking at the trend produced by changing the relative amount of the different materials, we observe that the increase in the plasmonic contribution dominates over the decrease of magnetic material. Higher antennas provide a stronger field enhancement, which results in more intense magneto-optical signal, even if it is produced by smaller nanoparticles. We thus conclude that the field enhancement produced by higher antennas compensates for the reduction of ferromagnetic material and that these hybrid structures are suitable to reduce the size of the magneto-optical active material without

the loss of the signal, thus obeying the technological need for dimensional scaling.

By experimenting with our new broadband, fast and sensitive spectrometer, we note that the response of these structures greatly depends on the geometry of the experiment, as a consequence of the different plasmonic response of the Au nanoantennas to it. The flexibility of these structures' response, in fact, allows them to be employed in various experiments with different requirements, by simply tuning their response by choosing the appropriate experimental geometry.

Finally, we conclude that a fast magneto-optical detection is possible, by implementing a parallel scan of the electromagnetic spectrum. The simplicity of this setup, which is very close to the original Faraday experiment, allows for a fast and highly sensitive magneto-optical detection in ambient conditions. Moreover, it enables also the characterization of optical properties within the same setup, by simply using different optics between light source and detector. This fact is of great importance when dealing with intertwined magneto-optical and optical properties which are also highly dependent on the experimental geometry.

Bibliography

[1] A. K. Zvezdin, V. A. Kotov, Modern Magnetooptics and Magnetooptical Materials, IOP Publishing Ltd, 1997.

[2] S. R. Woodford, A. Bringer, S. Blugel, Interpreting magnetization from faraday rotation in birefringent magnetic media, Journal of Applied Physics 101 (5).

[3] R. Wolfe, J. F. Dillon, R. A. Lieberman, V. J. Fratello, Broadband magneto-optic waveguide isolator, Applied Physics Letters 57 (10) (1990) 960–962.

[4] C. G. Stefanita, Magnetism: Basics and Applications, Springer, 2012.

[5] G. Armelles, A. Cebollada, A. García-Martín, M. U. González, Magnetoplasmonics: Combining magnetic and plasmonic functionalities (advanced optical materials 1/2013), Advanced Optical Materials 1 (1) (2013) 2–2.

[6] G. Armelles, A. Cebollada, A. García-Martín, J. M. García-Martín, M. U. González, J. B. González-Díaz, E. Ferreiro-Vila, J. F. Torrado, Magnetoplasmonic nanostructures: systems supporting both plasmonic and magnetic properties, Journal of Optics A: Pure and Applied Optics 11 (11) (2009) 114023.

[7] S. Polisetty, J. Scheffler, S. Sahoo, Y. Wang, T. Mukherjee, X. He, C. Binek, Optimization of magneto-optical kerr setup: Analyzing experimental assemblies using jones matrix formalism, Review of Scientific Instruments 79 (5).

[8] G. X. Du, S. Saito, M. Takahashi, Fast magneto-optical spectrometry by spectrometer, Review of Scientific Instruments 83 (1).

[9] T. V. Shahbazyan, M. I. Stockman, Plasmonics: Theory and Applications, Springer Netherlands, 2013.

[10] I. Freestone, N. Meeks, M. Sax, C. Higgitt, The lycurgus cup: a roman nanotechnology, Gold bulletin 40 (4) (2007) 270–277.

[11] M. Ashby, P. Ferreira, D. Schodek, Nanomaterials, Nanotechnologies and Design: An Introduction for Engineers and Architects, Butterworth-Hienemann, 2009.

[12] R. W. Wood, On a remarkable case of uneven distribution of light in a diffraction grating spectrum, Philisophical Magazine (1902) 4–396.

[13] G. Mie, Beirtrage zur optik truber medien, speziell kolloidaler metallosungen, Annalen der Physik (Leipzig) (1908) 25–37.

[14] D. Pines, D. Bohm, A collective description of electron interactions: 3. coulomb interactions in a degenerate electron gas, Physical Review (1953) 92–609.

[15] G. Armelles, J. B. González-Díaz, A. García-Martín, J. M. García-Martín, A. Cebollada, M. U. González, S. Acimovic, J. Cesario, R. Quidant, G. Badenes, Localized surface plasmon resonance effects on the magneto-optical activity of continuous au/co/au trilayers, Optics Express 16 (20) (2008) 16104–16112.

[16] S. A. Maier, Plasmonics: Fundamentals and Applications, Springer, 2007.

[17] E. Prodan, C. Radloff, N. J. Halas, P. Nordlander, A hybridization model for the plasmon response of complex nanostructures, Science 302 (5644) (2003) 419–422.

[18] K. Kneipp, Surface-enhanced raman scattering, Physics Today 60 (11) (2007) 40–46.

[19] S. Jiang, Surface enhanced raman scattering spectroscopy, Term Paper for Physics 598.

[20] M. E. Stewart, C. R. Anderton, L. B. Thompson, J. Maria, S. K. Gray, J. A. Rogers, R. G. Nuzzo, Nanostructured plasmonic sensors, Chemical Reviews 108 (2) (2008) 494–521.

[21] B. Sepulveda, A. Calle, L. M. Lechuga, G. Armelles, Highly sensitive detection of biomolecules with the magneto-optic surface-plasmon-resonance sensor, Optics Letters 31 (8) (2006) 1085–1087.

[22] A. Campion, P. Kambhampati, Surface-enhanced raman scattering, Chemical Society Reviews 27 (1998) 241–250.

[23] Y. Fu, J. Zhang, J. R. Lakowicz, Plasmon-enhanced fluorescence from single fluorophores end-linked to gold nanorods, Journal of the American Chemical Society 132 (16) (2010) 5540–5541.

[24] M. Faraday, Experimental researches in electricity. 19th series, Philosophical Transactions of the Royal Society of London 136 (1846) 1–20.

[25] J. Kerr, Xliii. on rotation of the plane of polarization by reflection from the pole of a magnet, Philosophical Magazine, 5th series 3 (19) (1877) 321–343.

[26] J. Kerr, Xxiv. on reflection of polarized light from the equatorial surface of a magnet, Philosophical Magazine, 5th series 5 (30) (1878) 161–177.

[27] P. N. Argyres, Theory of the faraday and kerr effects in ferromagnetics, Physical Review 97 (1955) 334–345.

[28] D. O'Connor, A. V. Zayats, Data storage: The third plasmonic revolution, Nature Nanotechnology 5 (2010) 482–483.

[29] J. Y. Chin, T. Steinle, T. Wehlus, D. Dregely, T. Weiss, V. I. Belotelov, B. Stritzker, H. Giessen, Nonreciprocal plasmonics enables giant enhancement of thin-film faraday rotation, Nature Communincations 4 (2013) 1599.

[30] J. Gonzalez-Diaz, Sepulveda, B. Garcia-Martin, G. A. Armelles, Cobalt dependence of the magneto-optical response in magnetoplasmonic nanodisks, Applied Physics Letters 97 (4) (2010) 043114–3.

[31] A. D. McNaught, A. Wilkinson (Eds.), IUPAC. Compendium of Chemical Terminology, 2nd ed. (the "Gold Book"), Blackwell Scientific Publications, Oxford (1997).

[32] T. K. Xia, P. M. Hui, D. Stroud, Theory of faraday rotation in granular magnetic materials, Journal of Applied Physics 67 (6) (1990) 2736–2741.

[33] U. K. Chettiar, A. R. Davoyan, N. Engheta, Hotspots from nonreciprocal surface waves, Optics Letters 39 (7) (2014) 1760–1763.

[34] P. Haefner, E. Luck, E. Mohler, Magnetooptical properties of surface plasma waves on copper, silver, gold, and aluminum, physica status solidi 185 (1) (1994) 289–2.

[35] B. Sepulveda, J. B. Gonzalez-Diaz, A. Garcia-Martin, L. M. Lechuga, G. Armelles, Plasmon-induced magneto-optical activity in nanosized gold disks, Physical Review Letters 104 (2010) 147401.

[36] T. Nikolajsen, K. Leosson, S. I. Bozhevolnyi, Surface plasmon polariton based modulators and switches operating at telecom wavelengths, Applied Physics Letters 85 (24) (2004) 5833–5835.

[37] M. J. Dicken, L. A. Sweatlock, D. Pacifici, H. J. Lezec, K. Bhattacharya, H. A. Atwater, Electrooptic modulation in thin film barium titanate plasmonic interferometers, Nano Letters 8 (11) (2008) 4048–4052.

[38] D. Pacifici, H. J. Lezec, H. A. Atwater, All-optical modulation by plasmonic excitation of cdse quantum dots, Nature Photonics 1 (7) (2007) 402–406.

[39] V. V. Temnov, G. Armelles, U. Woggon, D. Guzatov, A. Cebollada, A. Garcia-Martin, J.-M. Garcia-Martin, T. Thomay, A. Leitenstorfer, R. Bratschitsch, Active magneto-plasmonics in hybrid metal-ferromagnet structures, Nature Photoncs 4 (2) (2010) 107–111.

[40] C. Schafer, D. A. Gollmer, A. Horrer, J. Fulmes, A. Weber-Bargioni, S. Cabrini, P. J. Schuck, D. P. Kern, M. Fleischer, A single particle plasmon resonance study of 3d conical nanoantennas, Nanoscale 5 (2013) 7861–7866.

[41] K. Kumar, A. B. Dahlin, T. Sannomiya, S. Kaufmann, L. Isa, E. Reimhult, Embedded plasmonic nanomenhirs as location-specific biosensors, Nano Letters 13 (12) (2013) 6122–6129.

[42] H. Fredriksson, Y. Alaverdyan, A. Dmitriev, C. Langhammer, D. S. Sutherland, M. Zach, B. Kasemo, Hole mask colloidal lithography, Advanced Materials 19 (23) (2007) 4297–4302.

[43] S. Syrenova, C. Wadell, C. Langhammer, Shrinking-hole colloidal lithography: Self-aligned nanofabrication of complex plasmonic nanoantennas, Nano Letters 14 (5) (2014) 2655–2663.

[44] SILVER-Nova Super Range TE Cooled Spectrometers.
URL `http://www.stellarnet.us/products_spectrometers_SilverNova.htm`

[45] H. Czichos, T. Saito, L. Smith, Springer Handbook of Materials Measurement Methods, Springer handbooks, Springer, 2006.

[46] C. Graham, High-sensitivity magnetization measurements, Journal of Materials Science & Technology 16 (2) (2000) 97–101.